European Laboratory for Particle Physics

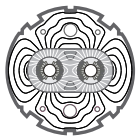

Large Hadron Collider Project

LHC Project Report 309

Radiation heating of primary collimators at ramping

I. Baishev[*,†], A.Barsukov[*,†] and J.B. Jeanneret

Abstract

A time-dependent temperature map is derived for the primary jaw of the momentum collimation system during the high transient loss period which is to occur at the beginning of the ramp of acceleration. An adequate margin factor is obtained for a loss of 5% of the nominal stored beam and for the nominal parabolic ramping curve.

[*]Institute for High Energy Physics, Protvino, Russia.
[†]Member of the Russian collaboration to the LHC Project.

Administrative Secretariat
LHC Division
CERN
CH-1211 Geneva 23
Switzerland

Geneva, 20 September 1999

1 Introduction

In LHC, the protons which are not captured by the RF system will not be accelerated and will be lost on a momentum collimation system soon after the beginning of the ramp of acceleration. The number of protons which are off the buckets can be large and the duration of the flash of the transient losses will be short, i.e. last approximately one second. The aim of this note is to derive a time-dependent three dimensional heat load map in the primary momentum collimator associated to these off-bucket protons.

We do our calculations for a fraction of the beam which is off-bucket $\Delta N_{\overline{RF}} = 5\%$ and for the nominal stored intensity $N_{stored} = 3\ 10^{14}$ protons.

Our derivation is made in three steps. We first analyse the 6D-motion of the off-bucket protons near the momentum cut made by the collimator and get a primary time-dependent impact map on the collimator (Section 2). We then develop hadronic showers in the collimator to produce a map of power deposition to which the primary ionisation of the impacting protons is added (Section 3). We then derive a semi-analytic model of heat diffusion in the collimator to get a time-dependent 3D map of temperatures (Section 4). We finally discuss the consequences for the design of the collimator, associated to the maximum temperature which can be reached in the collimator (Section 5).

2 Time-dependent impact map of the primary losses

2.1 Time structure of momentum losses at ramping

The off-bucket protons are lost at the beginning of the acceleration ramp. Their central relative momentum difference with respect to the accelerated central momentum increases with the time dependence [1]

$$|\delta_p(t)| = \frac{\delta p}{p} = \alpha t^2 \ . \tag{1}$$

The nominal value of α is chosen to control the 'snap-back' effect of the magnets [1] and is given in Table 1. The protons touch the primary momentum collimator when $|\delta_p(t)| = \delta_{cut} = 3 \cdot 10^{-3}$, a value fixed to match the momentum aperture of the LHC ring [2]. With (1), a proton with null initial momentum offset $\delta_p(0) = 0$ and null betatronic amplitude reaches δ_{cut} at time

$$t_o = \sqrt{\frac{\delta_{cut}}{\alpha}}. \tag{2}$$

With the conservative assumption that the initial momentum distribution is a δ-function at $\delta_p = 0$, the time distribution of the losses is fixed by the betatronic distribution of the beam. In a regime of slow enough ramping, protons with a large betatronic amplitude touch the collimator sooner than those with small betatronic amplitude. We make the likely hypothesis that the betatronic distribution of the beam is Gaussian with a rms size $\sigma_{\beta,x} = \sqrt{\epsilon\beta_x}$. With the slow transverse drift associated to the slow ramping, the betatronic distribution is cut on its two-sides simutaneously when approaching the collimator. The time distribution of the impacts is therefore the left side half of a Gaussian, or

$$f(t) = \frac{2\Theta(t_c - t)\Theta(t)}{\sqrt{2\pi}\sigma_t} \exp^{-(t-t_c)^2/2\sigma_t^2} \tag{3}$$

with $\Theta(t)$ the Heavyside function and t_c the time of the end of the process. To handle the process numerically we cut off the left tail of $f(t)$ at $2.5\sigma_t$, thus neglecting 1% of the

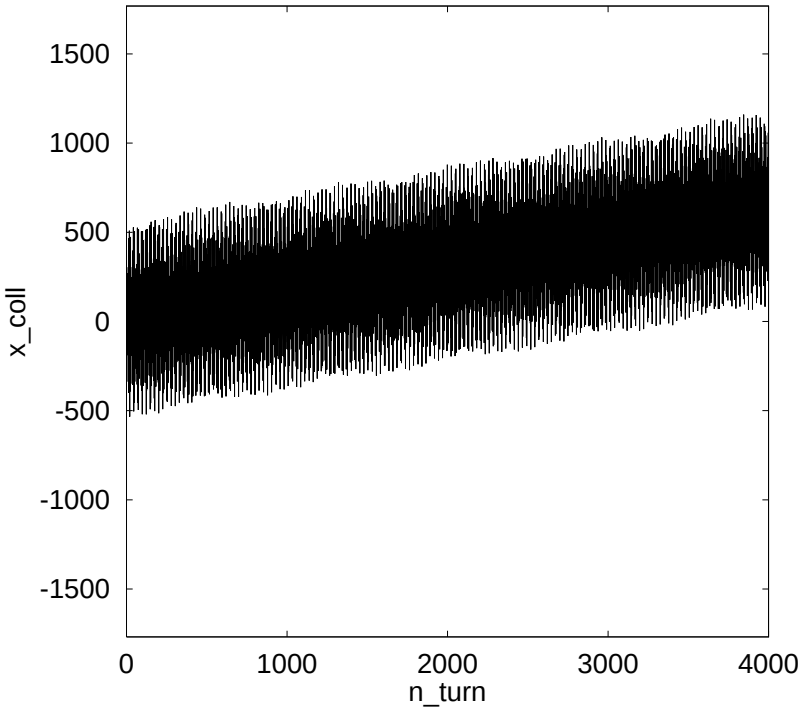

Figure 1: The horizontal betatronic motion combined with the drift associated to the acceleration for the protons which are off-bucket. In abscissa the turn number and in ordinate the horizontal position in micron with arbitrary origin. The drift speed is here $\dot{x} = 1.7\ 10^3\ \mu\text{ms}^{-1} = 0.15\ \mu$/turn, computed with 4 using the intermediate intermediate value $\alpha = 6 \cdot 10^{-5}\ \text{s}^{-2}$ of Table 1.

energy deposition and fix $t_c = 2.5\sigma_t$ to start the process at $t = 0$. The rms of $f(t)$ is $\sigma_t = \sigma_{\beta,x}/\dot{x}$ with $\dot{x} = d(D\delta_p)/dt = d(D\alpha t^2))/dt = 2D\alpha t$ computed at $t = t_o$ and the dispersion D at the primary collimator. With

$$dotx(t = t_o) = 2D\sqrt{\alpha\delta_{cut}}, \tag{4}$$

$$\sigma_t = \frac{1}{2D}\sqrt{\frac{\epsilon\beta_x}{\alpha\delta_{cut}}}. \tag{5}$$

We used $D = 2$ m , $\beta = 100$ m at injection, and the nominal emittance $\epsilon = .0078\pi$ mm·mrad.

2.2 Impact parameter distribution on the primary collimator

The impact parameter distribution is obtained by combining the smearing of the betatron amplitude to the drift in the horizontal plane associated to the growth of $|\delta_p(t)|$. Sixtrack tracking data for LHC Version 6.-2 were provided to us by F. Schmidt [3]. Protons of betatronic amplitudes $A_x = A_y = 1\ \sigma_{\beta,x}$ and fixed relative momentum offset $\delta_p = 2{\cdot}10^{-3}$ were tracked over N=4000 turns. At each turn the 6 coordinates were recorded. Two seeds of the LHC machine were used, a 'good' and an 'average' one, where 'good' and 'average' qualify their respective dynamic aperture near the edge of the bucket. To the horizontal betatronic excursion $x_{\beta,i}$ at turn i the quantity $D|\delta_p(t_i)|$ is added, with $t_i = i/f_r$ and f_r the frequency rotation of the beam. An exemple is shown in Figure 1. With i growing, the

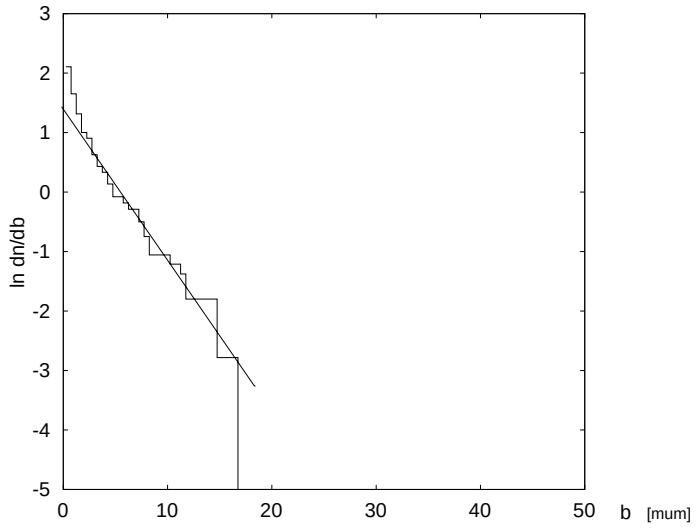

Figure 2: Simulated impact parameter distribution for the average seed (see text). An exponential function fits quite well the data, except near $b = 0$.

quantity $x_i = x_{\beta,i} + D|\delta_p(t_i)|$ is compared to the former largest value $x_j = x_{\beta,j} + D|\delta_p(t_j)|$. When $x_i > x_j$, the impact parameter distribution is added the contribution

$$\frac{dN}{db} = \frac{dN}{db} + \frac{\Theta(x - x_j)\Theta(x_i - x)}{i - j} \tag{6}$$

with b the impact parameter and $\Theta(x)$ the Heavyside function. The function (6) reflects the fact that the collimator can occupy randomly any position between two consecutive maxima of x. Only one impact can occur between two consecutive maxima, justifying the relative weight $1/(i - j)$. For three ramping speeds and for the two seeds (see Table 1), the impact parameter distribution is well approximated by an exponential function $dn/db = a\exp(-kb)$ truncated at some impact parameter b_{max}, see an exemple in Figure 2. The result of the fit of the k values is given in Table 1. As it can be expected, the b distribution is steeper for small ramping speeds, but with a quite weak dependence on α. Contrary to what might be expected, the seed qualified as being good at $\delta_p < \delta_{bucket}$ has a more shaky motion at $\delta_p = 3 \cdot 10^{-3}$. A small deviation at low b values will be taken into account by keeping the slope k as fitted, but multiplying the number of lost protons by a correction factor

$$c_{corr} = \frac{dn}{db}(b = 0)_{tracking} / \frac{dn}{db}(b = 0)_{fit}. \tag{7}$$

For every value of α, we will use the steepest of the two distributions, i.e. the k values of the average seed, see Table 1. To simplify the parametrisation of the time-dependant impact map, we use the same correction to the normalisation as fixed by the largest deviation observed , i.e. the case displayed in Figure 2 for which $c_{corr} = 1.9$.

2.3 Vertical distribution of impacting protons

With the hypothesis of uncoupled betatronic motion, the vertical distribution of impacting protons is simply given by the vertical betatronic distribution, a Gaussian distribution of rms width $\sigma_{\beta,y} = \sqrt{\epsilon\beta_y} = 0.88$ mm with $\beta_y = 100$ m. The vertical distribution

Table 1: The parameter k as a function of the ramp speed α and for the two seeds 'average' and 'good'. The first value of α is the nominal one. The two other ones correspond to worse cases, for which the duration of the flash of losses is shorter, as shown in Table 2.

α [s^{-2}]	$k_{average}$ [μm^{-1}]	k_{good} [μm^{-1}]
$6 \cdot 10^{-6}$	0.25	0.13
$6 \cdot 10^{-5}$	0.19	0.14
$6 \cdot 10^{-4}$	0.10	0.09

Table 2: Input parameters for the time dependant impact parameter distribution as a function of the ramp speed α. Typical impact parameters are given by the quantity b_o.

α [s^{-2}]	σ_t [s]	k [μm^{-1}]	$b_o = 1/k$ [μm]
$6 \cdot 10^{-6}$	1.65	0.25	4.0
$6 \cdot 10^{-5}$	0.52	0.19	5.2
$6 \cdot 10^{-4}$	0.165	0.10	10

is then

$$\frac{dn}{dy} = \frac{1}{\sqrt{2\pi}\sigma_y} \exp^{-y^2/2\sigma_y^2} \tag{8}$$

2.4 Longitudinal distribution of impacting protons

In the worst case for energy deposition, the longitudinal distribution of impacts is a δ-function at the entrance face of the jaw and does not appear explicitely in the overall time-dependent distribution. This impact distribution is the input for further propagation of the protons in the jaw. In a good approximation, the longitudinal distribution of energy deposition is the sum of hadronic showers developed in the collimator and of the primary ionisation of the impacting protons along their path.

2.5 Time-dependent impact parameter distribution

Combining (3),(6) and (8), we get the factorised time-dependent impact parameter distribution

$$\frac{d^3N(t,b,y)}{dtdbdy} = \frac{c_{corr}\Delta N_{loss} k\Theta(t_c - t)\Theta(t)}{\pi\sigma_t\sigma_y} e^{-(t-t_c)^2/2\sigma_t^2} e^{-kb} e^{-y^2/2\sigma_y^2}, \tag{9}$$

with b the impact parameter (and also the horizontal coordinate with its origin at the inner face of the jaw), y the vertical coordinate and $t_c = 2.5\sigma_t$ to cut off the infinitely long tail of a Gaussian.

3 Energy deposition

We do our calculations in the local Cartesian system (x, y, z) attached to the collimator jaw. The coordinate x coincides with the horizontal impact parameter b and y

Table 3: Additional parameters for the time dependant distribution .

ΔN_{loss}	$1.5 \cdot 10^{13}$ protons
c_{corr}	1.9
σ_y	0.88 mm

and z are the vertical and the longitudinal coordinates respectively. The collimator jaw occupies the box :

$$0 \leq x \leq X\,,\ -Y \leq y \leq Y\,,\ 0 \leq z \leq L\,,$$

where $X = 3.5$ cm, $Y = 3.2$ cm and $L = 20$ cm. The jaw material is aluminium.

An estimation of the density of energy deposition at the entrance of the jaw (x=0, y=0, z=0) is obtained by multiplying the beam density (9) by the ionization energy loss (6.1 MeV/cm for 450 GeV proton). The result is a very impressive peak energy in the range of hundreds kJ/cm^3. But this value cannot be used for realistic estimations of the jaw temperature because of the relatively long duration of the proton pulse which allows heat to diffuse far from the zone of the heat deposition. We must also consider the additional component of energy deposition associated to the protons-nuclear interactions in the jaw. We compute a 3D-map of energy deposition per protons $q(x, y, z)$ including this effect and then deduce a time integrated map $Q(x, y, z) = c_{corr}\Delta N_{loss} q(x, y, z)$ (see next alinea). The time-dependent power deposition map $P_V(x, y, z, t)$ is obtained by using Equation (9) in which all the time-independent terms are replaced by $Q(x, y, z)$. This is allowed by the fact that the energy deposition of each proton is done in a time of the order of its time-of-flight through the jaw, much smaller than our time-scale fixed by σ_t. We therefore use

$$P_V(x, y, z, t) = Q(x, y, z) f(t) \quad \text{with} \quad f(t) = \sqrt{\frac{2}{\pi}}\,\frac{1}{\sigma_t}\,\Theta(t_c - t)\Theta(t) e^{-(t-t_c)^2/2\sigma_t^2} \qquad (10)$$

To consider thermal diffusion we must first compute the map of heat deposition $Q(x, y, z)$ everywhere in the jaw. Protons deposit energy first by primary ionisation. Then successive interactions which produce many secondary particles deposit again energy also by ionisation. This process (the 'hadronic shower') is simulated by a Monte-Carlo method using the code MARS [4]. The important feature of the present calculations is that a special algorithm for the particle tracking near the surface of the material is enabled for precise description of the 'edge scattering' of the primary protons. The energy deposition density is determined as the energy absorbed inside the predefined space cell divided by the cell volume so that

$$Q(x, y, z) = q_{ijl},\ \text{at}\ \ x \in [x_i, x_{i+1}],\ y \in [y_j, y_{j+1}],\ z \in [z_l, z_{l+1}]\ . \qquad (11)$$

The cell dimensions vary from ($\Delta x = 1\mu$m, $\Delta y = 1$mm, $\Delta z = 5$mm) at small (x, y, z) to ($\Delta x = 1$cm, $\Delta y = 1$cm, $\Delta z = 3$cm).

As can be seen from (9) the incident beam density is a monotonically increasing function of t. Therefore the maximum temperature must be expected at $t = t_c$. The y-distribution is a gaussian centered at $y = 0$, thus $Q(x, y, z)$ is y-symmetric, has a local maximum at $y = 0$ and a crest line along $(x, 0, z)$. The plots of $Q(x, 0, z)$ are presented

in Figure 3 for the minimum and the maximum values of the ramp speed α. $Q(x,0,z)$ is found to be a monotonically decreasing function of x for every z. Unfortunately the same is not true for the z-dependence which is decreasing at very small x but increasing at bigger x. While the largest energy deposition is $Q(0,0,0)$, it is therefore not necessarily the case for the temperature. We must seek for the maximum temperature by analyzing its dependence on z at x=0, y=0 and $t = t_c$.

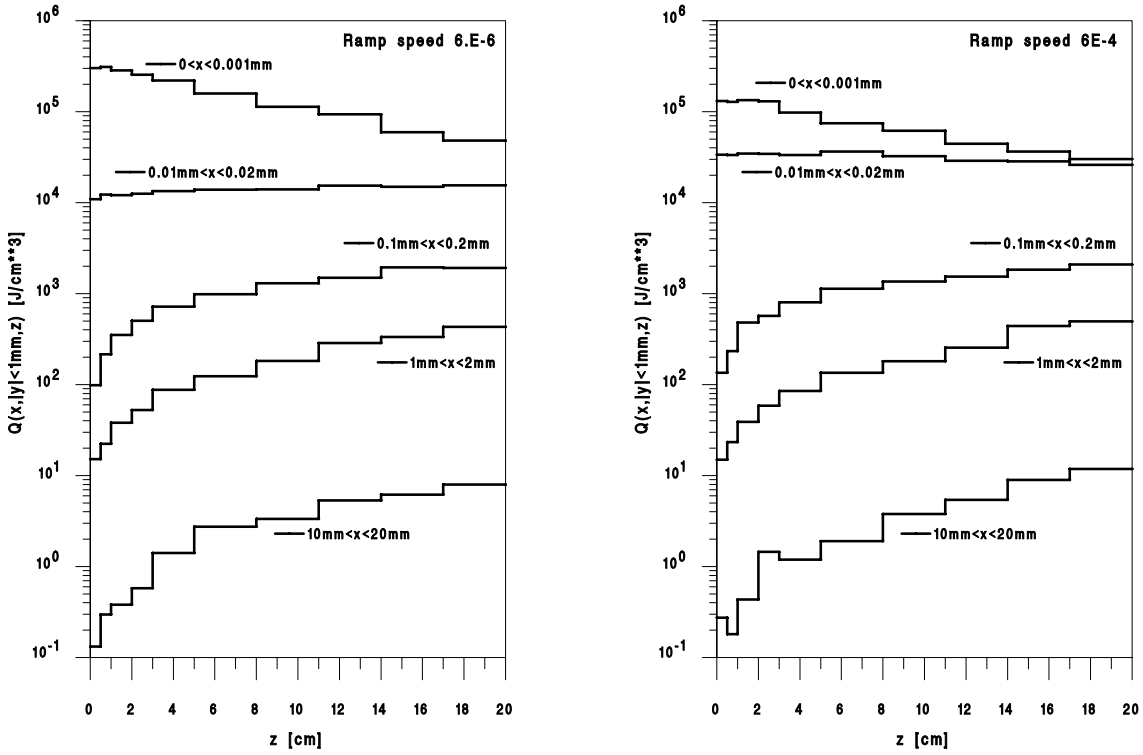

Figure 3: Energy deposition density in the collimator jaw. The ramp speed α [s^{-2}] is shown in the right upper corner of each frame.

4 Thermal calculations

4.1 Solution of thermal conductance equation

To obtain the temperature distribution $T(x,y,z,t)$ in the jaw material with thermal conductivity λ , specific heat C and density ρ, the heat conduction equation

$$\frac{\partial T}{\partial t} - \frac{\lambda}{\rho\, C}\left(\frac{\partial^2 T}{\partial x^2} + \frac{\partial^2 T}{\partial y^2} + \frac{\partial^2 T}{\partial z^2}\right) = \frac{1}{\rho\, C}\, P_V(x,y,z,t)\ , \tag{12}$$

must be solved for $P_V(x,y,z,t)$ taken from (10) and for a set of boundary and initial conditions related to the design of the collimator.

The collimator jaw is situated in a vacuum box. It is driven by the outside motor through the gear and the supporting rod. One of the rod ends is connected to the jaw and the another one is connected to the outside gear. If thermal radiation is neglected then five out of six jaw surfaces can be considered as thermally insulated. The conditions at the surface $x = X$ are more complicated because a part of it is in a good thermal contact

with the outside. They can be simplified if the heat diffusion length

$$< d >= \sqrt{\frac{\lambda t_c}{C\rho}}$$

is less than X. With the numerical constants $\lambda = 2.4$ W/(cm·K), $C = 1$ J/(g·K), $\rho = 2.7$ g/cm^3 for the aluminium jaw and the longest pulse duration $t_c = 4.1$ s we get $< d > = 1.9$ cm. It is less than $X = 3.5$ cm and any reasonably simple condition at $x = X$ will not affect much the calculated temperature maximum.

We used the following set of boundary and initial conditions

$$\begin{cases} \frac{\partial T}{\partial x}(0, y, z, t) = 0 \\ \\ \frac{\partial T}{\partial y}(x, \pm Y, z, t) = 0 \\ \\ \frac{\partial T}{\partial z}(x, y, 0, t) = 0, \ \frac{\partial T}{\partial z}(x, y, L, t) = 0 \\ \\ T(X, y, z, t) = T_0 \\ \\ T(x, y, z, 0) = T_0 \end{cases} \tag{13}$$

where T_0 is the room temperature.

The solution of the equation (12) with the conditions (13) is found as the Fourier series

$$T(x, y, z, t) - T_0 =$$

$$= \frac{4}{C\,\rho\,XYL} \sum_{n=0}^{\infty} \sum_{m=0}^{\infty} \sum_{k=0}^{\infty} e^{-\xi_{nmk}\,t}\, I_{nmk}(t)\, J_{nmk}\, \cos(\alpha_n\, x)\, \cos(\beta_m\, y)\, \cos(\gamma_k\, z)\ , \tag{14}$$

$$I_{nmk}(t) = \int_0^t f_t(\tau)\, e^{\xi_{nmk}\,\tau}\, d\tau, \tag{15}$$

$$J_{nmk} = \int_0^X \int_0^Y \int_0^L Q(x, y, z)\, \cos(\alpha_n\, x)\, \cos(\beta_m\, y)\, \cos(\gamma_k\, z) dx\, dy\, dz\ . \tag{16}$$

The parameters in (14), (15) and (16)

$$\alpha_n = \frac{\pi\, n}{2\, X},\ \beta_m = \frac{\pi\, m}{Y},\ \gamma_k = \frac{\pi\, k}{L},\ \xi_{nmk} = \frac{\lambda}{\rho\, C}\left(\alpha_n^2 + \beta_m^2 + \gamma_k^2\right)$$

are determined by satisfying the boundary conditions (13).

The integrals in (15) and (16) are calculated numerically. With $Q(x, y, z)$ made discrete in (11), the integration of (16) is reduced to triple summations over (i, j, l). The cosine terms in (16) are integrated analytically into the cells. The convergence of the triple series (14) was studied by trial computations. A truncation of the series at $n_{max} = 300,\ m_{max} = 60,\ k_{max} = 30$ was found sufficient to provide an accuracy of 3% for the maximum temperature.

4.2 Temperature maximum

In the course of the calculations a monotonic increase of T with z was found with the maximum at $z = L$ for any time t. The results of $T(0, 0, z, t)$ calculations are presented in Figures 4-6 as functions of t at $z = 0$, $L/2$ and L for each of three ramp speeds. All the curves have the sharp maxima at $t = t_c$ as it was expected. Their left side ($t < t_c$) is similar to a Gaussian while the right side ($t > t_c$) is rather similar to an exponential.

The absolute maximum $T_{max} = T(0, 0, L, t_c)$ increases with the ramp speed α, see Table 4. To ensure reliable operation, the temperature excursion in aluminum shall not be larger then $\Delta T \simeq 200$ K [5]. This limit is respected for the two slow ramping speeds that we studied. For the nominal one, the margin factor is ~ 4, which is a quite comfortable value.

Table 4: The temperature maximum T_{max} in the jaw as a function of the ramp speed α and considering that $\Delta N = 1.5\ 10^{13}$ protons are captured, or 5% of a stored beam of nominal intensity.

α [s^{-2}]	$\Delta T = T_{max} - T_0$ [K]
$6 \cdot 10^{-6}$	52
$6 \cdot 10^{-5}$	120
$6 \cdot 10^{-4}$	260

Knowing the temperature maximum obtained by considering only the diffusion of heat, we can estimate the possible influence of the neglected thermal radiation on our results. Using the Stefan-Boltzmann law of black body radiation we can express the maximum irradiated power as

$$P_{rad} = S_{eff}\sigma(T_{max}^4 - T_0^4),$$

where $\sigma = 5.67 \cdot 10^{-12}$ W/(cm$^2K^4$) is the Stefan-Boltzmann constant. Taking $S_{eff} = 6\sigma_y L$, $T_0 = 300$ K and $T_{max} = 560$ K we get P_{rad}= 5.4 W. Let us compare it with the average power deposition

$$P_{dep} = \Delta N_{loss}\Delta E_{abs}/t_c,$$

where ΔE_{abs} is the energy absorbed in the jaw per one incident proton. It is equal approximately to 600 MeV at any α. Taking $t_c = 0.41$ s which corresponds to $T_{max} = 560$ K used in the calculation of P_{rad} we get $P_{dep} = 3500$ W which is much higher than P_{rad}. Therefore thermal radiation is negligible in our case.

We estimate the effect of multiturn absorption on the primary collimation to about 8% of the result obtained with only the primary pass of the protons. This marginal factor is obtained by computing the secondary flux leaving the primary jaw as $f_{sec} = \exp^{-L/\lambda_{abs}} = 0.5$ with the length of the jaw $L = 20$ cm and $\lambda_{abs} = 39.4$ cm. The secondary flux is scattered by multiple coulomb scattering and populates a 2D-Gaussian distribution of r.m.s width $\theta = (1.5\ 10^{-3}/p[\text{GeV/c}]) \times (L/L_R)^{1/2}$ with the radiation length $L_R = 8.9$ cm and the beam momentum p. Normalised to the beam divergence, this width is $\theta_{mcs}/\sigma' = 5$. We use this last number as an approximate dilution factor in phase-space, of which only one σ escapes the secondary collimators (the secondary jaws are retracted by one σ with respect to the primar ones). We therefore get a ratio of the multiturn flux to the primary one of approximately $f_{sec}/5 = 0.08$.

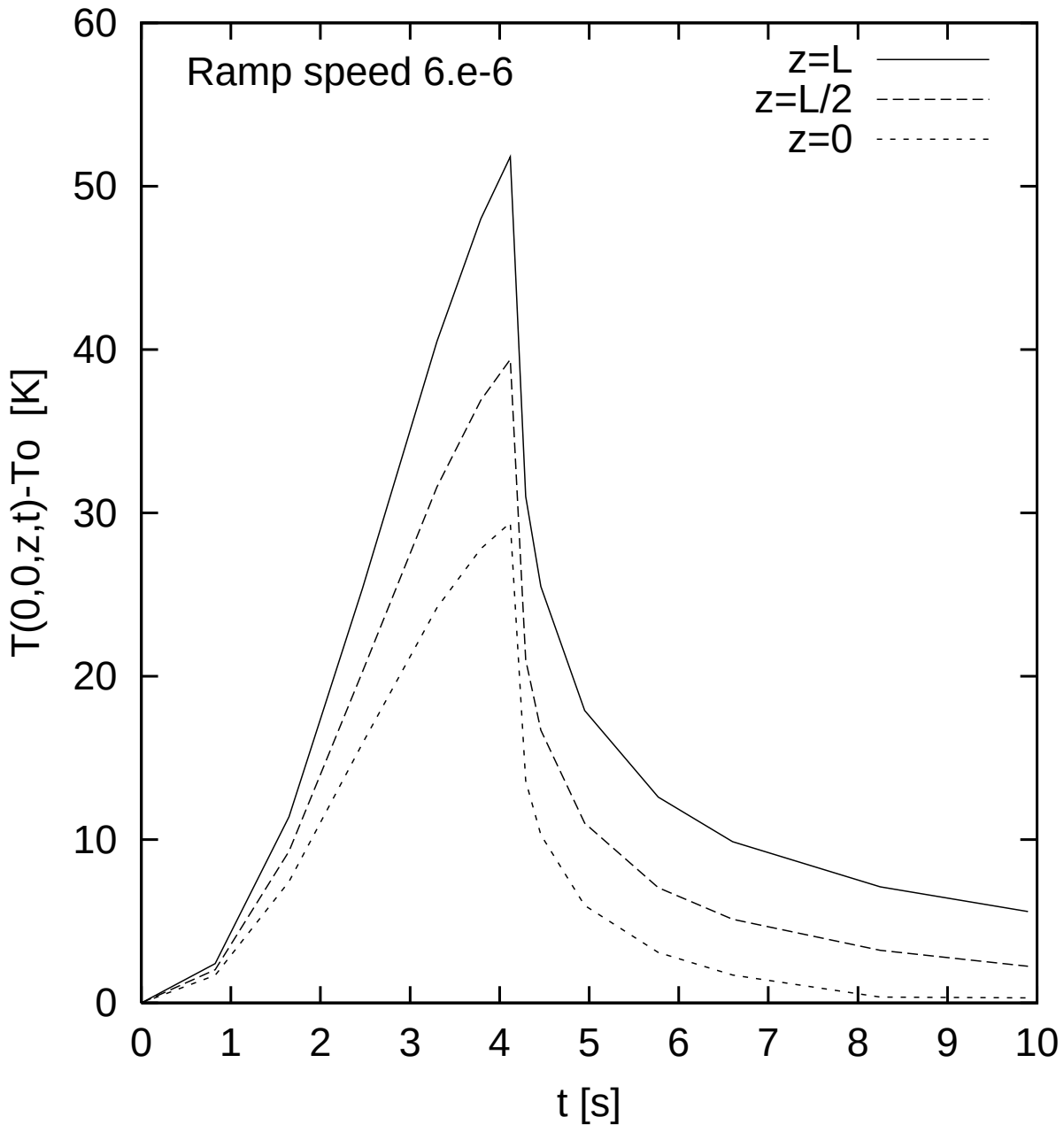

Figure 4: Time dependence of the temperature in the collimator jaw for three longitudinal positions z. The ramp speed α [s^{-2}] is shown in the upper left corner of the frame.

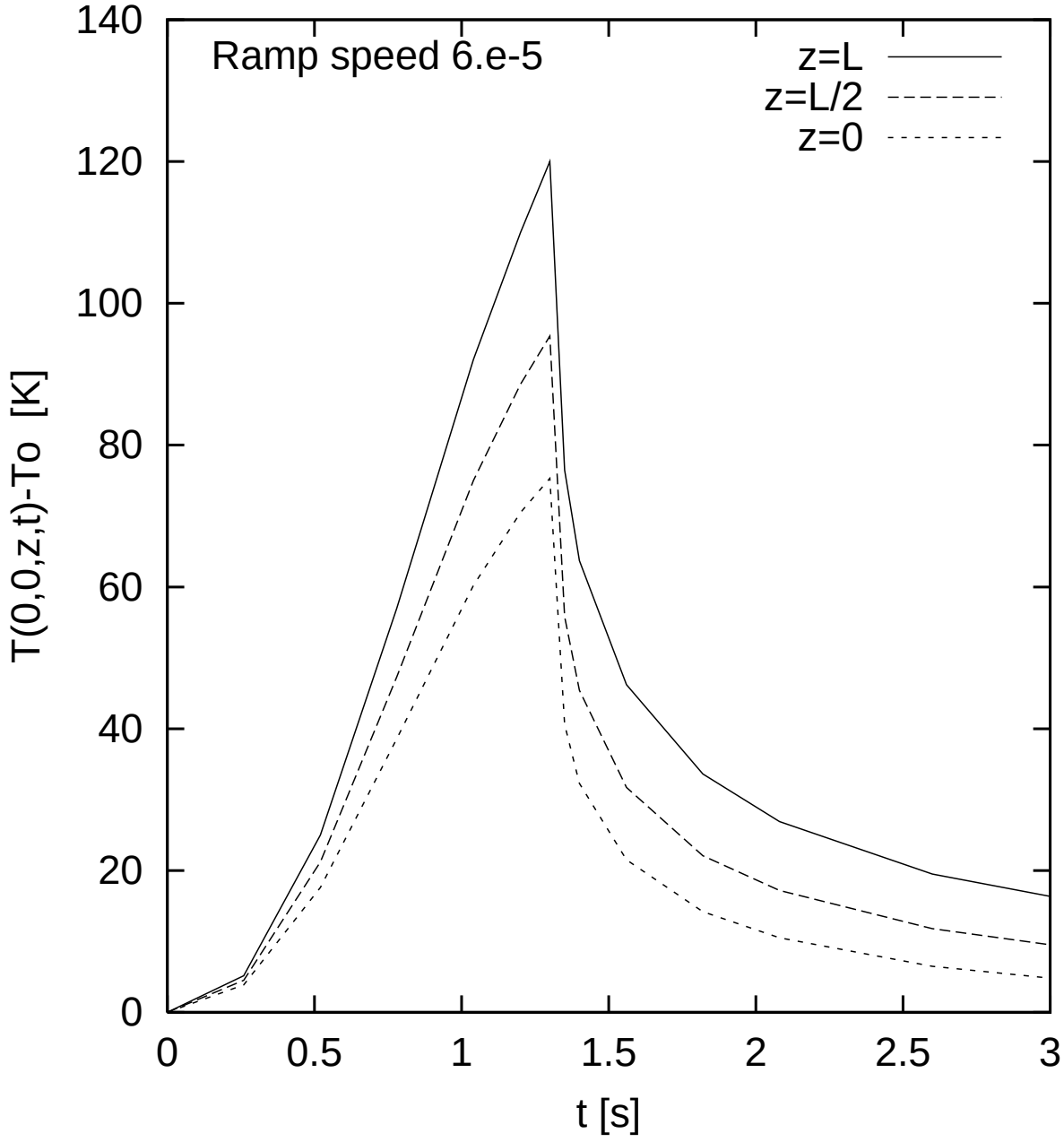

Figure 5: The same as Fig. 4 for $\alpha = 6 \cdot 10^{-5}$ s^{-2}

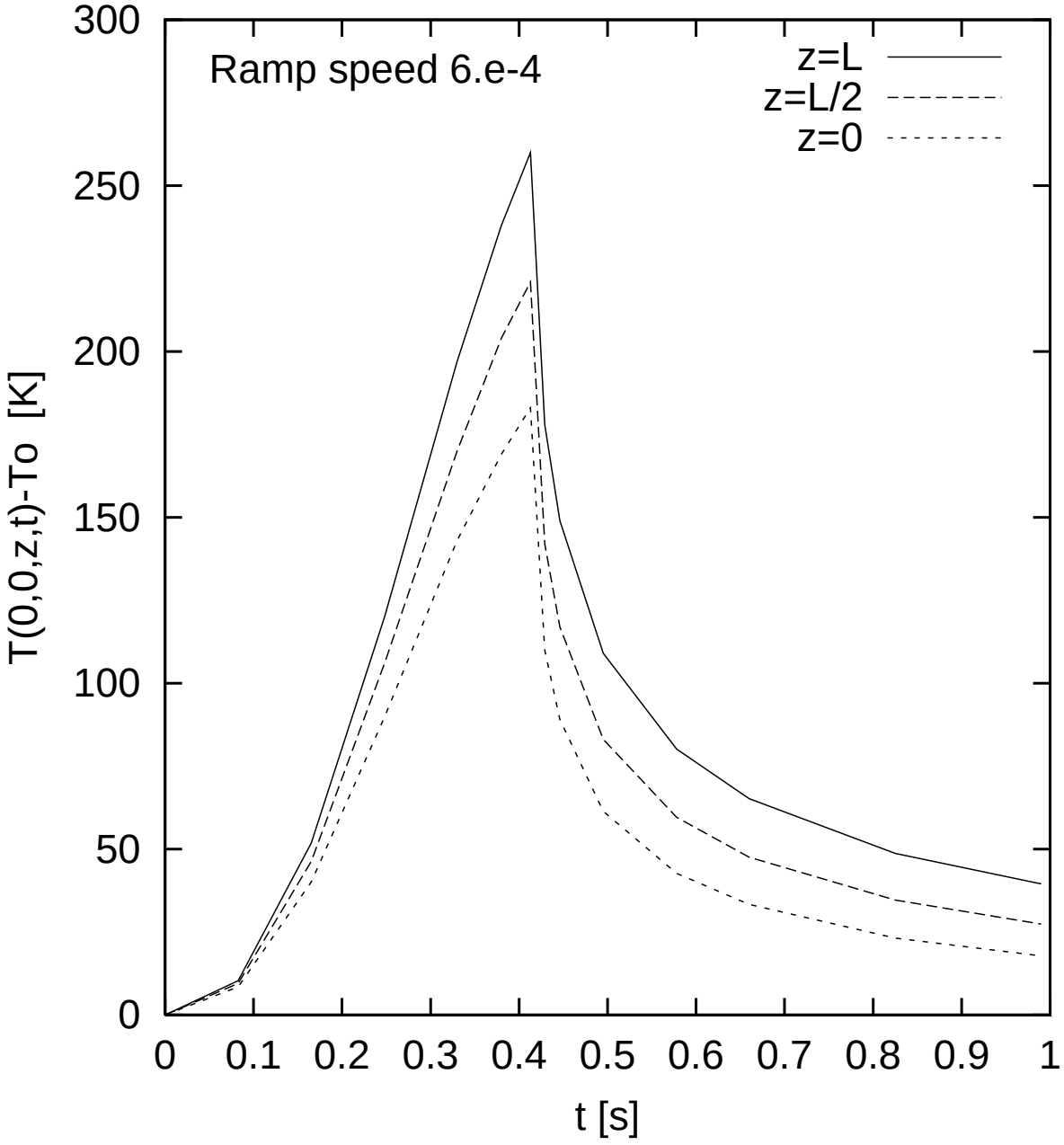

Figure 6: The same as Fig. 4 for $\alpha = 6 \cdot 10^{-4}$ s^{-2}

The x-gradient of the temperature will serve to estimate the thermal expansion of the jaw towards the beam axis as well as to compute internal stress in the jaw. The results of $T(x, 0, z, t_c)$ calculations are presented in Figures 7-9 at $z = 0$, $L/2$ and L for each of three ramp speeds. Unlike the energy deposition $Q(x, 0, z)$, the temperature curves have a flat top at $x \leq 0.5$ mm and the volume where $T \approx T_{max}$ has a finite size.

5 Discussion

If we consider that the fraction of the stored LHC beam which lies outside the RF buckets is smaller than 5%, then with the nominal ramping speed of acceleration the temperature in the primary jaw of the momentum collimation system would not increase by more than 50 °C, or a factor four below the critical temperature offset.

Would faster initial segment of the ramp be considered, the margin goes down and becomes marginal for a ramp coefficient 100 times larger than the nominal value.

The ultimate stored current of LHC is 1.6 times larger than the nominal one. In this case our margin factor drops down to about two.

With these adequate but not outstanding margin factors, a real time control of the level of losses at the primary jaw must be used and connected to the beam abort system to ensure the integrity of the collimators.

Acknowledgements

We thank Frank Schmidt who provided us with the proton tracking data without which we would had no realistic input material for this study. One of us (IB) is grateful to J. Gareyte and F. Ruggiero who invited him in the SL/AP group and therefore allowed this study to be made. We also thank G. Stevenson, K. Potter and the direction of the LHC Project for providing an efficient frame to the collaboration between CERN and the IHEP laboratory.

References

[1] L. Bottura, P. Burla and R. Wolf, CERN LHC Proj.Rep.172, March1998.
[2] J.B. Jeanneret, Phys.Rev. ST Accel and Beams, **1**, 081001, December 1998.
[3] F. Schmidt, private communication, June 1999.
[4] I.L.Azhgirey, I.A.Kurochkin and V.V.Talanov, in: Ann. of XV Conf. on Charg. Part. Accel., p.74, Protvino, 22-24.10.96 (in russian).
[5] R. Jung, private communication, September 1999.

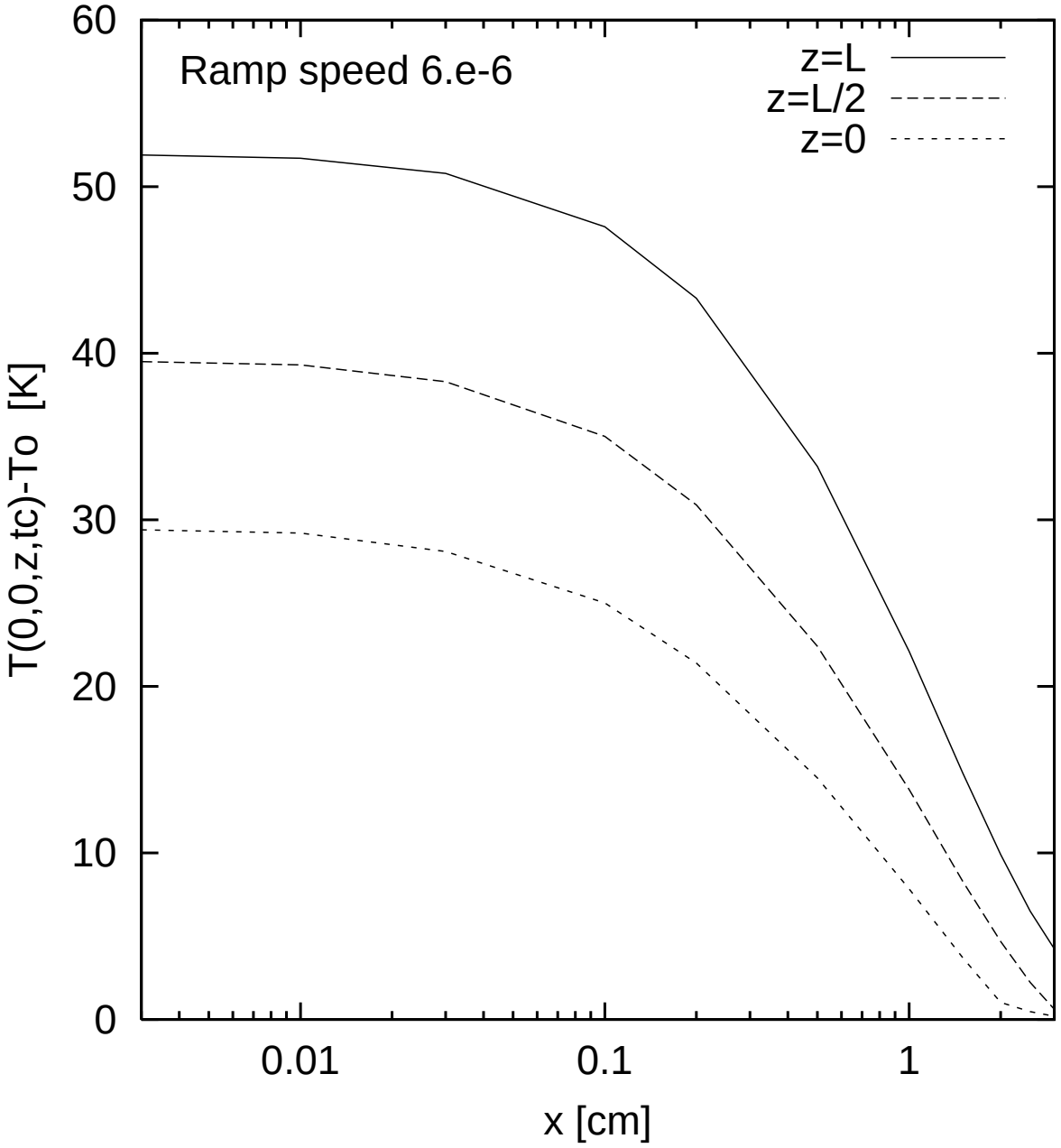

Figure 7: Horizontal distribution of the temperature in the collimator jaw at the end of the proton pulse t_c for three longitudinal positions z. The ramp speed α [s^{-2}] is shown in the upper left corner of the frame.

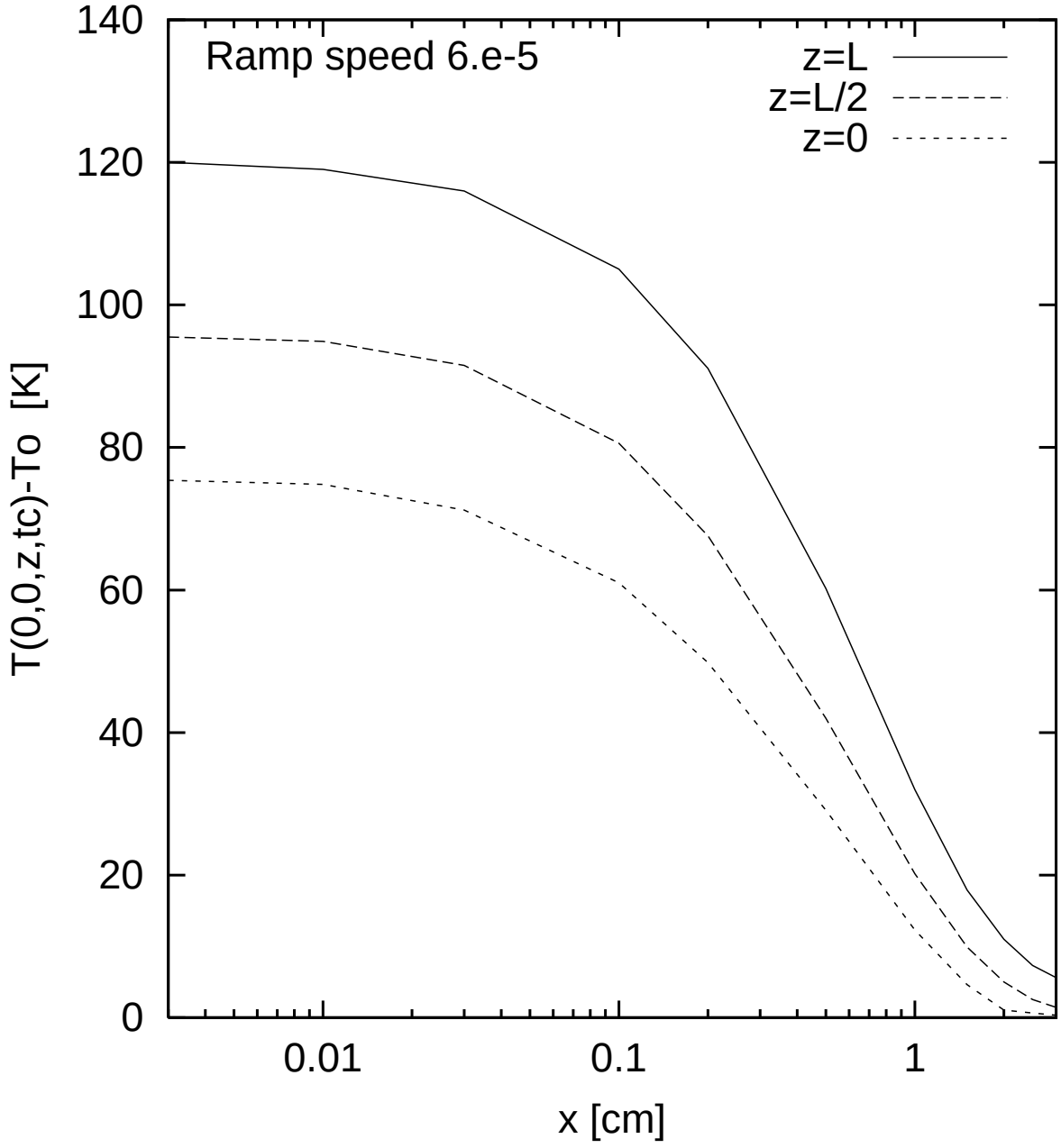

Figure 8: The same as Fig. 7 for $\alpha = 6 \cdot 10^{-5}$ s^{-2}

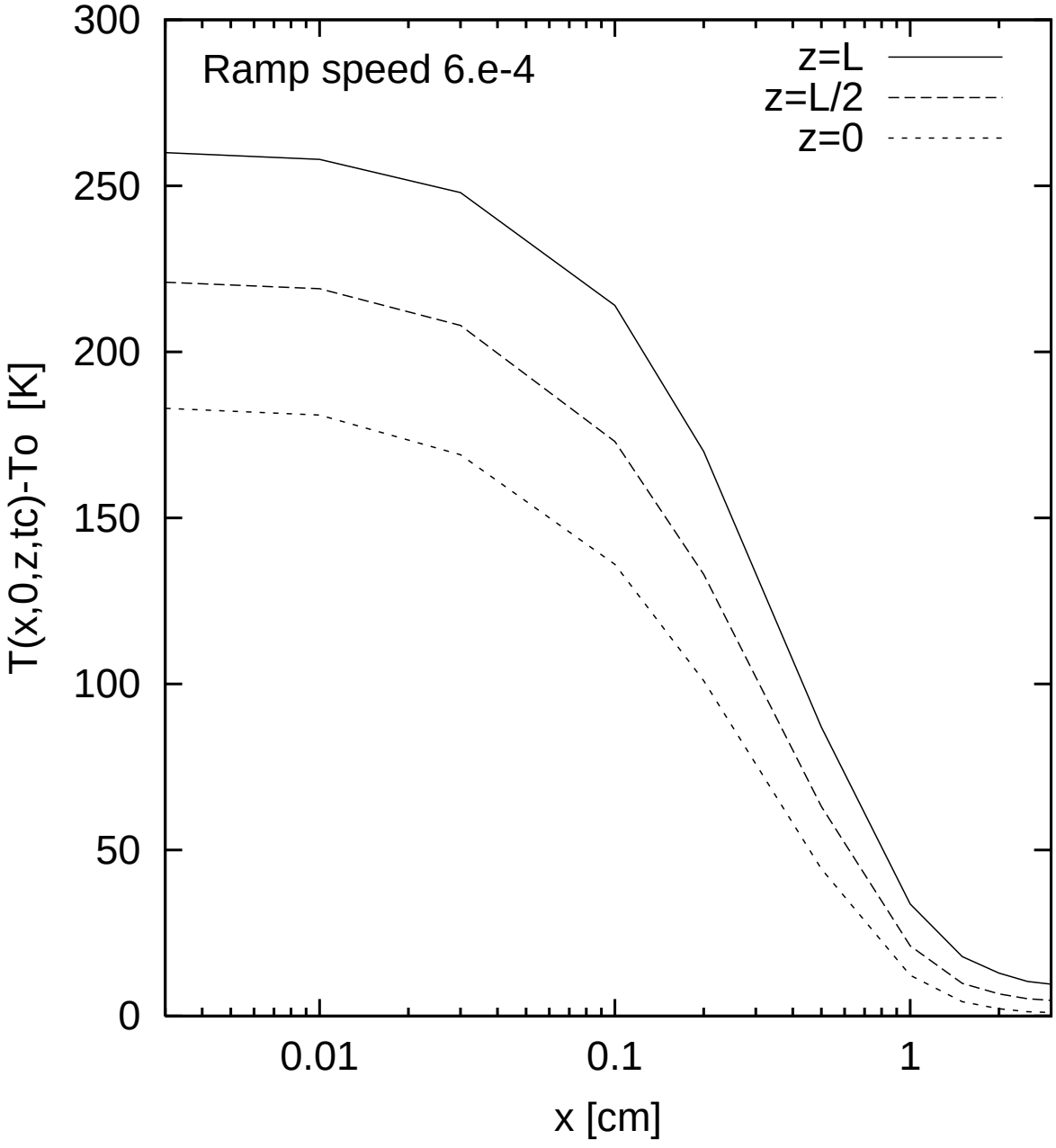

Figure 9: The same as Fig. 7 for $\alpha = 6 \cdot 10^{-4}$ s^{-2}